

## Article

# Using 3D Ray Tracing Technology to Study the Disturbance Effect of Rocket Plume on Ionosphere

Qingfeng Li <sup>\*</sup>, Zeyun Li and Hanxian Fang 

College of Meteorology and Oceanography, National University of Defense Technology, Changsha 410073, China; lizeyun@nudt.edu.cn (Z.L.); fanghx@hit.edu.cn (H.F.)

\* Correspondence: lqf123@nudt.edu.cn

**Abstract:** In this paper, the initial neutral atmospheric parameters, background ionospheric parameters and geomagnetic field parameters of the ionosphere are obtained by NRLMSISE-00 model, IRI-2016 model and IGRF-13 model, respectively. Considering the neutral gas diffusion process, ion chemical reaction and plasma diffusion process, a three-dimensional dynamic model of chemical substances released by rocket plume disturbing the ionosphere is constructed. The influence of the disturbance on the echo path of high frequency radio waves with different incident frequencies is simulated by using three-dimensional digital ray-tracing technology. Using this model, the process of ionospheric disturbance caused by the main chemical substances H<sub>2</sub> and H<sub>2</sub>O in the rocket plume under three different release conditions: fixed-point release at 300 km, vertical path at 250–350 km and parabolic path at 250–350 km, and the influence of the ionospheric cavity on the radio wave propagation of high frequency radio waves at different frequencies are simulated. The main purpose of the article is to focus on the effect of the cavity generated by the rocket exhaust on the propagation of radio waves. It mainly studies the perturbation effect on the ionosphere under different release conditions, considers the neutral gas diffusion process, ion chemical reaction and plasma diffusion process, and establishes the three-dimensional dynamics of the ionospheric electron density and the spatiotemporal distribution of the plume plasma learning model. Finally, the three-dimensional ray-tracing algorithm is used to simulate the propagation path of the radio wave through the disturbance area. We considered three different release conditions, including fixed-point release, vertical path and parabolic path. The ionospheric disturbances produced by these different releases are compared and analyzed, and their effects on the propagation path of radio waves are studied.

**Keywords:** artificial; influence on ionosphere; rocket plume; ionospheric cavity; ray tracing



**Citation:** Li, Q.; Li, Z.; Fang, H. Using 3D Ray Tracing Technology to Study the Disturbance Effect of Rocket Plume on Ionosphere. *Atmosphere* **2022**, *13*, 1150. <https://doi.org/10.3390/atmos13071150>

Received: 13 June 2022

Accepted: 19 July 2022

Published: 20 July 2022

**Publisher's Note:** MDPI stays neutral with regard to jurisdictional claims in published maps and institutional affiliations.



**Copyright:** © 2022 by the authors. Licensee MDPI, Basel, Switzerland. This article is an open access article distributed under the terms and conditions of the Creative Commons Attribution (CC BY) license (<https://creativecommons.org/licenses/by/4.0/>).

## 1. Introduction

The ionosphere is an important link in the solar–terrestrial space environment. There is a large amount of plasma in it, which can affect the propagation trajectory of electromagnetic waves by causing it to reflect, refract or scatter, and cause special effects such as rotation of the polarization plane. In addition to natural disturbance factors such as solar flares and magnetic storms, man-made products from human activity in space such as rocket plumes will inevitably interfere with the ionosphere. Rocket plume is a kind of plasma with high temperature, nonmagnetization and weak ionization. After rocket launch, a large number of chemicals will be emitted. Their main components are H<sub>2</sub>, H<sub>2</sub>O, CO<sub>2</sub> and Al<sub>2</sub>O<sub>3</sub>, which will be converted into gas at high temperature. When the rocket plume is released into the ionosphere, a large number of neutral gas molecules will be injected into the ionosphere. The corresponding electron density in the background ionosphere will be greatly reduced to form an "artificial ionospheric hole", which is the main physical mechanism of chemical release to produce an "ionospheric hole". When the Vanguard II spacecraft was launched in 1959, Booker (1961) first observed the existence of ionospheric holes by using a ground-based ionosonde; these holes were repeatedly observed in subsequent rocket launches [1].

Mendillo et al. reported that when the sky laboratory of NASA was launched into space by Saturn V rocket in 1973, it caused large-scale loss of F region. Using ATS-3 and ATS-5 geostationary satellites, it was observed that a large electron density depletion region, namely ionospheric cavity, was formed at an altitude of 300 km. The electron density decreased by 50% or more, and the disturbance radius reached 1000 km. The duration of this disturbance was about 4 hours. The incident caused a short-wave communication interruption accident over the vast area of the Atlantic Ocean, and the minimum reflection frequency was reduced to about 2 MHz [2,3]. Mendillo et al. (1975) assumed and analyzed the causes of the formation of ionospheric holes and gave the possible factors for their gradual disappearance. Its research showed that there were a large number of oxygen ions (O<sup>+</sup>) in the F region of the background ionosphere. Oxygen ions had a violent ion–atom exchange reaction with neutral gas molecules in the rocket plume to form molecular ions, and then immediately reacted with electrons in the background ionosphere, resulting in the reduction of electron ion concentration and the formation of huge ionospheric holes.

Zinn et al. [4] reported that when the High Energy Astrophysical Observatory Satellite (HEAO-C) was launched in 1979, the release of chemical substances at an altitude of 410 km was  $1.6 \times 10^7$  mol/s, the rocket plume emitted by the rocket interacts with the ionospheric plasma, resulting in a large electron density cavity 40 km thick in the ionospheric F layer with a north–south span of 600–800 km. Savastano et al. [5] used the real-time TEC observation data obtained from the dual frequency GEO satellite to describe the physical characteristics of ionospheric plasma density loss caused by the launch of Falcon 9 rocket at Vandenberg Air Force Base in California in 2017.

Three-dimensional ray-tracing technology [6,7] is one of the most effective methods to describe and analyze the echo propagation path of high frequency radio waves. Ray tracing methods mainly include analytical ray tracing [8–11] and numerical ray tracing [12–14]. Although the analytical ray-tracing speed is fast, it is difficult to obtain the corresponding analytical solution when considering the influence of geomagnetic field, and the numerical ray-tracing technology can solve this problem. Zhou et al. [15] established the traveling ionospheric disturbance (TID) model caused by atmospheric gravity wave according to the ionospheric quasi parabola model, and on the basis of this model, the influence of 3D ray-tracing technology on high frequency radio wave coordinate registration (CR) is analyzed. The ionospheric cavity formed by the rocket plume has a great impact on the high-frequency radio wave propagation of high frequency radio waves [16]. In this study, the process of ionospheric disturbance was caused by the main chemical substances H<sub>2</sub> and H<sub>2</sub>O in the rocket plume under three different release conditions: fixed-point release of 300 km, vertical path of 250–350 km and parabolic path of 250–350 km is simulated, as well as the influence of the ionospheric cavity on the radio wave propagation of different frequencies of high frequency radio waves.

## 2. Kinetic Model

The study of ionospheric disturbances and gases released by the rocket plume is the basis for building dynamic models. In the ionosphere, the dynamic process of the gas ejected from the rocket tail flame is extremely complicated, including thermal expansion, cooling, gasification, free diffusion, and inertial motion. In this paper, the dynamic process after the equilibrium of diffusion is simulated, including the chemical reaction with the upper atmosphere material and the process of plasma diffusion.

### 2.1. Neutral Gas Diffusion

When the rocket plume is released in the early stage of the background ionosphere, the neutral gas molecules in the plume will push the surrounding plasma away like a snow blower under the high pressure of the thrusters [17,18]. The continuity equation and momentum equation of neutral gas can be described as

$$\frac{\partial n}{\partial t} + \nabla \cdot (n \vec{v}) = P - L + S \quad (1)$$

$$\frac{d\vec{v}}{dt} = \vec{g} - k \frac{\nabla(nT)}{nm} + \omega_a (\vec{w} - \vec{v}) \tag{2}$$

The representative meanings of the relevant parameters in the formula are shown in the following Table 1.

**Table 1.** The meaning of related parameters of the above Formulas (1) and (2).

Number	Parameter	Representation
1	$n$	Neutral gas number density
2	$\vec{v}$	Neutral gas velocity
3	P	Production rate of chemical substances
4	L	Chemical loss rate
5	S	Gas primitive function
6	m	Molecular mass of released gas
7	$\vec{g} = -g\vec{z}$	Acceleration of gravity
8	$\vec{z}$	Vertically upward unit vector
9	T	Gas temperature
10	$\vec{w}$	Neutral gas drift velocity
11	$\omega_a$	Collision frequency
12	k	Boltzmann constant

It is assumed that the background of the ionosphere and thermosphere is horizontally stratified, ignoring the motion of the background atmosphere, the thermal diffusion effect of neutral molecules and the expansion process of chemical substances, and considering the effects of chemical reaction loss and gravity. The selected Cartesian coordinate system takes the neutral gas release point as the center, the x-axis points to the East, the y-axis points to the North, and the z-axis points vertically upward. Then the approximate solution of the diffusion equation of neutral gas under the condition of point source release is as follows [19]:

$$n_i(r, z, t) = \frac{N_0}{(4\pi D_0 t)^{3/2}} \exp \left[ -(z - z_0) \left( \frac{3}{4H_a} + \frac{1}{2H_i} \right) - \alpha t \right. \\ \left. - \frac{H_a^2 \{1 - \exp[-(z - z_0)/(2H_a)]\}^2}{4D_0 t} - \frac{r^2 \exp\left[-\frac{z - z_0}{(2H_a)}\right]}{4D_0 t} \right. \\ \left. - \left( \frac{1}{H_a} - \frac{1}{H_i} \right)^2 \frac{D_0 t \cdot \exp[(z - z_0)/(2H_a)]}{4} \right] \tag{3}$$

The meanings of the letters in the formula are shown in Table 2.

**Table 2.** The meaning of related parameters in the above Formula (3).

Number	Parameter	Representation $\text{cm}^3 \cdot \text{s}^{-1}$
1	$n_i(r, z, t)$	Number density of neutral gas
2	$z_0$	Height of release point
3	$N_0$	The amount of neutral gas molecules
4	$H_a = kT/(m_a g)$	Atmospheric elevation
5	$H_i = kT/(m_s g)$	Elevation of the released gas
6	k	Boltzmann constant

**Table 2.** Cont.

Number	Parameter	Representation $\text{cm}^3 \cdot \text{s}^{-1}$
7	T	Background gas temperature
8	$m_a$	Atmospheric average molecular weight
9	$m_s$	Release the molecular weight of neutral gas
10	g	Acceleration of gravity
11	$\alpha t$	Loss item caused by chemical reaction

If only O, O<sub>2</sub> and N<sub>2</sub> in the background atmosphere are considered, the expression of the diffusion coefficient of chemical substances H<sub>2</sub> and H<sub>2</sub>O at the release point is as follows [20]:

$$D_{H_2} = \left( \frac{N(O)}{2.97 \times 10^{18} T^{0.5}} + \frac{N(N_2)}{2.8 \times 10^{17} T^{0.74}} + \frac{N(O_2)}{3.06 \times 10^{17} T^{0.732}} \right)^{-1} \text{cm}^2/\text{s} \quad (4)$$

$$D_{H_2O} = \left( \frac{N(O)}{8.46 \times 10^{17} T^{0.5}} + \frac{N(N_2)}{2.04 \times 10^{17} T^{0.623}} + \frac{N(O_2)}{2.02 \times 10^{17} T^{0.632}} \right)^{-1} \text{cm}^2/\text{s} \quad (5)$$

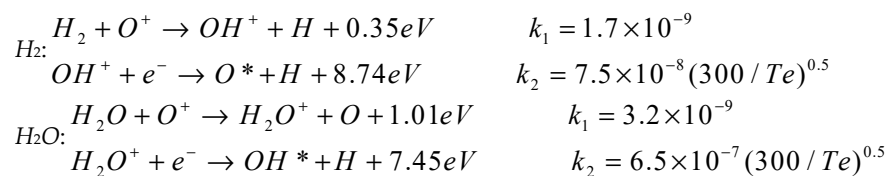
In the case of point source, the density distribution function of the release is  $n(x,y,z,t)$ . Assuming that the same amount of neutral gas is released at any release point on the rocket flight trajectory, the approximate solution of the diffusion equation of neutral gas in the case of multi-source release is obtained as follows [21]:

$$n_D(x,y,z,t) = \int_0^t \iiint n(x-\alpha, y-\eta, z-\lambda, t-\gamma) d\alpha d\eta d\lambda d\gamma \quad (6)$$

where  $n_D$  is the distribution function of release density under multi-source release;  $(\alpha, \eta, \lambda, \gamma)$  is the point on the release path. In numerical simulation, multi-source release can be regarded as a system composed of multiple discrete release point sources. By modulating the temporal and spatial distribution of each release point source, different ionospheric hole shapes are obtained.

### 2.2. Ion Chemical Reaction Process

There are a lot of oxygen atom ions in the F layer of the ionosphere and the recombination coefficient between a and electrons is about  $10^{-12} \text{cm}^3 \cdot \text{s}^{-1}$ . However, neutral gas can easily convert atoms into molecules, and the recombination coefficient can reach  $10^{-7} \text{cm}^3 \cdot \text{s}^{-1}$  or even greater, which is about five orders of magnitude greater than that between O+ and electrons [2,22]. Therefore, it can consume a lot of electrons in the ionosphere and form artificial ionospheric holes. The main chemical reaction equation after the release of neutral gas molecules H<sub>2</sub> and H<sub>2</sub>O is



where  $k_1$  and  $k_2$  are chemical reaction coefficients and  $Te$  is electron temperature. The reduction of electron density is

$$\Delta n_e = k_2 \cdot (k_1 \cdot n_{H_2O} \cdot n_{O^+} \cdot \Delta t) \cdot n_e \cdot \Delta t \quad (7)$$

### 2.3. Plasma Diffusion

The continuity equation of plasma is

$$\frac{\partial n_p}{\partial t} = -\nabla \cdot (n_p v_p) + P - L \tag{8}$$

The specific meaning of each parameter in the above formula is shown in the following Table 3.

**Table 3.** The meaning of related parameters in the Formula (8).

Number	Parameter	Representation
1	$n_p$	The number density of the plasma (mainly refers to O+)
2	$P_p$	Plasma generation rate
3	$L_p$	Plasma loss rate
4	$v_p$	The drift velocity of the plasma parallel to the direction of the magnetic field

where the plasma velocity  $v_p$  along the geomagnetic lines is

$$v_p = -D \left[ \frac{\partial \ln n_p T_p}{\partial s} + \frac{\sin I}{H_p} \right] + v_D \tag{9}$$

where  $D$  is the effective bipolar diffusion coefficient,  $D = (1 + T_i/T_e)D_i$ , and  $D_i$  is the ion diffusion coefficient [23];  $T_p$  is the plasma temperature,  $T_p = (T_i + T_e)/2$ ;  $H_p$  is the elevation of plasma,  $H_p = 2kT_p/(m_p g)$ ; and  $I$  is the magnetic inclination. Because we assume that the plasma only drifts along the magnetic field direction, the continuity equation is rewritten as  $v_D$  is the additional drift speed (wind speed), the influence of which is ignored in this article. Substituting it into the above formula can produce the plasma diffusion equation [21]:

$$\begin{aligned} \frac{\partial n_p}{\partial t} = & D \cos^2 I \frac{\partial^2 n_p}{\partial y^2} + D \frac{\cos I \sin I}{H_p} \frac{\partial n_p}{\partial y} - v_D \cos I \frac{\partial n_p}{\partial y} \\ & + D \sin^2 I \frac{\partial^2 n_p}{\partial z^2} + \left( \sin^2 I \frac{\partial D}{\partial z} + D \frac{1}{T_p} \sin^2 I \frac{\partial T_p}{\partial z} + D \frac{1}{H_p} \sin^2 I - v_D \sin I \right) \frac{\partial n_p}{\partial z} \\ & + \left( \frac{1}{T_p} \sin^2 I \frac{\partial D}{\partial z} \frac{\partial T_p}{\partial z} + \frac{1}{H_p} \sin^2 I \frac{\partial D}{\partial z} + D \sin^2 I \frac{\partial^2 \ln T_p}{\partial z^2} + D \sin^2 I \frac{\partial \left( \frac{1}{H_p} \right)}{\partial z} \right) n_p + P_p - L_p \end{aligned} \tag{10}$$

The specific meaning of each parameter in the above formula is shown in the Table 4 below.

**Table 4.** The meaning of related parameters in the above Formula (10).

Number	Parameter	Representation
1	$n_p$	The number density of the plasma (mainly refers to O+)
2	$D = \left(1 + \frac{T_e}{T_i}\right) D_i$	Effective bipolar diffusion coefficient
3	$D_i$	Ion diffusion coefficient
4	$T_p = (T_e + T_i)/2$	Plasma temperature
5	$H_p = 2KT_p/(m_p g)$	The elevation of plasma
6	$P_p$	Plasma generation rate
7	$L_p$	Plasma loss rate

2.4. D Ray Tracing

Haselgrove [12] derived the Hamiltonian (or canonical) equation of the ray path of high-frequency radio waves propagating in the ionosphere. In this article, we use the Runge–Kutta method to numerically solve the Haselgrove ray square differential equation, and use variable step size technology to ensure the calculation speed. Assuming that the earth is a sphere, the established three-dimensional coordinate diagram is shown in Figure 1.

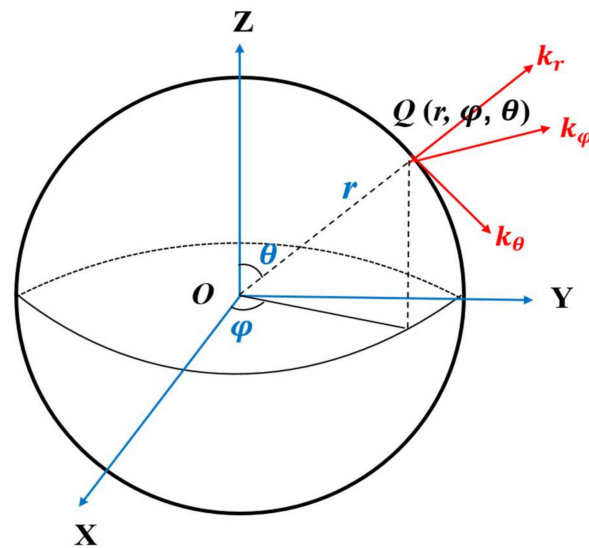


Figure 1. Schematic diagram of ray-tracing spatial coordinates.

The meaning of each letter in Figure 1 is shown in Table 5.

Table 5. The meaning of related parameters in the above Figure 1.

Number	Parameter	Representation
1	Point O	Geocentric position
2	OXYZ	Cartesian coordinate system
3	OXY	Equatorial plane
4	OX	Point to 0° longitude
5	OY	Point to 90°E
6	OZ	Point to the North Pole along the axis of the earth
6	$(r, \varphi, \theta)$	The coordinate position of Q
7	r	The distance from point Q to the center of the earth
8	$\varphi$	The offset angle of the longitude of OX to Q point eastward
9	$\theta$	Complementary angle of Q point latitude
10	$\vec{k} = (k_r, k_\varphi, k_\theta)$	Wave vector at point Q
11	$k_r$	Vertical ground up
12	$k_\varphi$	Pointing to the geographical true east
13	$k_\theta$	Pointing to the geographic direction due south

The ray-tracing equation is solved based on the above coordinate system. Haselgrove equations are as follows:

$$\left\{ \begin{aligned} \frac{dr}{dP'} &= \frac{c}{\omega} k_r \\ \frac{d\theta}{dP'} &= \frac{c}{\omega r} k_\theta \\ \frac{d\varphi}{dP'} &= \frac{c}{r\omega \sin \theta} k_\varphi \\ \frac{dk_r}{dP'} &= -\frac{\omega}{2c} \frac{\partial X}{\partial r} + k_\theta^2 \frac{c}{r\omega} + k_\varphi^2 \frac{c}{r\omega} \\ \frac{dk_\theta}{dP'} &= \frac{1}{r} \left( -\frac{\omega}{2c} \frac{\partial X}{\partial \theta} - k_r k_\theta \frac{c}{\omega} + k_\varphi^2 \frac{c}{\omega} \cot \theta \right) \\ \frac{dk_\varphi}{dP'} &= \frac{1}{r \sin \theta} \left( -\frac{\omega}{2c} \frac{\partial X}{\partial \varphi} - k_\theta k_r \frac{c}{\omega} \sin \theta + \frac{c}{\omega} k_\theta k_\varphi \cos \theta \right) \end{aligned} \right. \quad (11)$$

The meaning of each letter in Formula (10) is shown in Table 6.

**Table 6.** The meaning of related parameters in the above Formula (11).

Number	Parameter	Representation
1	$P'$	The group path
2	$c$	The speed of light
3	$\omega = 2 \pi f$	The angular frequency of the radio wave
4	$f$	The frequency of the radio wave
5	$\omega_{pe}$	The angular frequency of the plasma
6	$n = \sqrt{1 - X}$	Refractive index

In the table above,  $X = \omega_{pe}^2 / \omega^2$ , where  $\omega_{pe}$  is the plasma angular frequency. This system of equations partially simplifies the Appleton Hartree equation and takes into account the refractive index  $n = \sqrt{1 - \frac{\omega_{pe}^2}{\omega^2}}$ . When we consider the flight of the rocket, the neutral gas released by the rocket plumes cannot be released only at a single point at a fixed height. Therefore, in the ray-tracing equation, we consider the dynamic process of the release of neutral gas from multiple sources; that is, the released neutral gas changes with time and space. At the same time, when the rocket is flying, the release area of the plumes' chemical substances will also be affected by the magnetic field, electric field, etc., so in the ray-tracing equation, we also need to consider the effect of the magnetic field force.

The initial emission conditions of radio wave are determined as emission position  $(r_0, \varphi_0, \theta_0)$ , azimuth  $\alpha$ , elevation  $\beta$ , and the radio wave frequency  $f$ , etc. The initial value of the ray differential equation can be obtained, as shown in the following formula:

$$\left\{ \begin{aligned} r &= r_0 \\ \theta &= \frac{\pi}{2} - \lambda_0 \\ \varphi &= \varphi_0 \\ k_r &= \left| \vec{k} \right| \cos\left(\frac{\pi}{2} - \beta\right) = \frac{\omega}{c} \sin \beta \\ k_\theta &= -\left| \vec{k} \right| \cos \beta \cos \alpha = -\frac{\omega}{c} \cos \beta \cos \alpha \\ k_\varphi &= \left| \vec{k} \right| \cos \beta \cos\left(\frac{\pi}{2} - \alpha\right) = \frac{\omega}{c} \cos \beta \sin \alpha \end{aligned} \right. \quad (12)$$

To sum up, starting from the initial value, the ray coordinate value and wave vector component after each step can be calculated by advancing according to the appropriate step of the group path  $P'$ . Finally, all ray coordinates are connected to obtain the image of ray trajectory.

On the one hand, we assume that the background of the ionosphere and the thermosphere is a horizontal layered distribution when establishing the dynamic model, while ignoring the motion of the background atmosphere, the thermal diffusion effect of neutral

molecules and the expansion process of chemical substances. On the other hand, due to the disturbance of the rocket tail flame, the change of the electron density in the area where the tail flame chemical substances are released destroys the density distribution structure of the original charged particles and breaks the original dynamic balance. Affected by magnetic field, electric field, ion and electron density gradient, collision of ionospheric disturbance zone, neutral wind, etc., the plasma will drift, and its detailed force situation is more complicated, but in the F region of the ionosphere, the cyclotron frequency of ions is much larger than the collision frequency of ion–ion and ion–neutral molecules, so we assume that the plasma moves only along the magnetic field lines; that is, we only consider the most influential force (magnetic field force) effect. This will also lead to some relative errors in our model, which is also the limitation of the current model. With the follow-up in-depth research, we will try to improve the performance of the model to achieve a smaller error.

### 3. Experimental Simulation and Parameter Setting

In this paper, the neutral atmospheric parameters are obtained by NRLMSISE-00 model. The background ionospheric parameters are obtained by international reference ionospheric 2016 (IRI-2016) model, and the geomagnetic field parameters are obtained by IGRF13 model. The release point and ray emission point are set in the mid-latitude city, Nanjing (119° E, 32° N), and the simulated release time is 1 July 2010. The numerical simulation platform is matlab R2019b.

Firstly, the neutral atmosphere and background ionospheric parameters in the release region are obtained by the empirical models: NRLMSISE-00, IRI-2016 and IGRF-13. The spatial distribution of the neutral gas molecules ejected in the plume is obtained by using the diffusion equation. Then, the change of electron density in the release region can be determined by the ion chemical reaction equation and the conditions of  $\sum N_i \approx N_e$  of quasi neutral characteristic of plasma. Then, the time step is further advanced, and the above cycle is repeated to obtain the electron density at the next time, and the time step is 1.0 s. After obtaining the temporal and spatial distribution of neutral gas and electron density, the 3D digital ray-tracing method can be used to simulate the impact of chemical release on the high-frequency radio wave echo path. In this paper, a fast algorithm is used for short-wave ray-tracing, and the group path step size is adjusted adaptively according to the gradient of plasma frequency. The elevation range of simulated short wave is 75°~105°, and the elevation progressive step is 2°. It is transmitted eastward by default; that is, the azimuth is 90°.

### 4. Simulation Results and Discussion

#### 4.1. Disturbance Released by H<sub>2</sub> in Different Paths and Its Influence on Radar Wave Propagation Path

##### 4.1.1. Simulation of Spatial Distribution of H<sub>2</sub> after Release and Diffusion in Different Paths

The ionospheric cavity formed by H<sub>2</sub> under three different release conditions and its influence on radar wave propagation are simulated. Firstly, we simulated the release of 3000 mol H<sub>2</sub> at a fixed altitude of 300 km. Then, we assume that when the rocket flies at a speed of about 10 km/s, 3000 mol H<sub>2</sub> is released every 0.5 s from 250 km to 350 km in the vertical direction; that is, 3000 mol H<sub>2</sub> is released every 5 km in the vertical rising path; Finally, we simulated the release of 3000 mol H<sub>2</sub> every 5 km in the parabolic path from 250 km to 350 km under the same flight conditions.

As shown in Figure 2, after releasing H<sub>2</sub> for 100 s according to 300 km fixed-point release, 250–350 km vertical path release and 250–350 km parabolic curve path, the released substance H<sub>2</sub> has different spatial distribution characteristics. At the fixed-point release of 300 km, the release diffuses far in the east-west direction and less in the vertical height direction, resulting in a flat ellipsoidal release space; When released at a vertical path of 250–350 km, the East-West diffusion of the release is smaller than the vertical diffusion, resulting in a slender cylindrical diffusion space with narrow bottom and wide top; When

released at the parabolic path of 250–350 km, a parabolic tubular release space is generated. Three different release paths produce different diffusion spaces. After 100 s of release, the maximum diffusion radius of  $H_2$  concentration in the order of  $10^6 \text{ cm}^{-3}$  and above reaches 88 km, and the maximum concentration of  $H_2$  after 100 s of release is  $4.8 \times 10^7 \text{ cm}^{-3}$ .

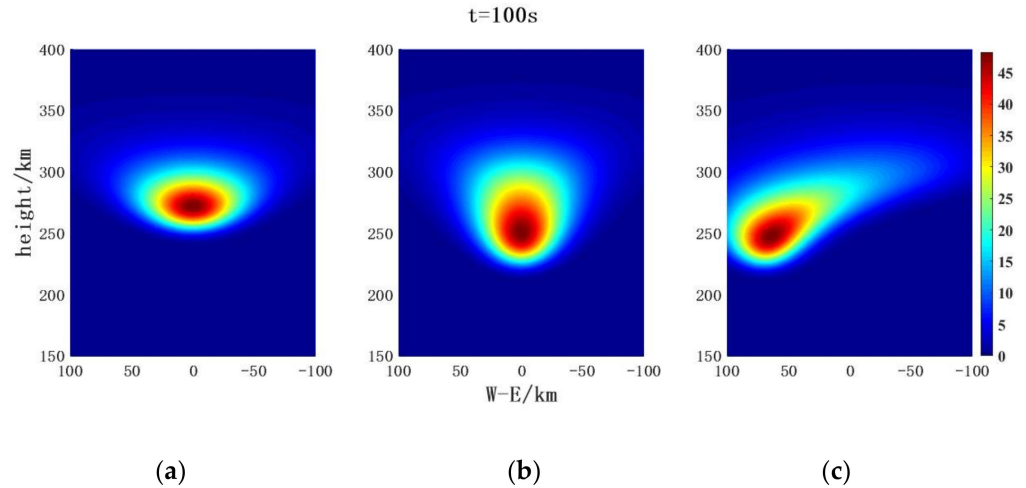


**Figure 2.** Spatial distribution of  $H_2$  released by rocket after releasing  $H_2$  for 100 s under different flight paths (electron density unit:  $10^6 \text{ cm}^{-3}$ ): (a) 300 km fixed-point release (b) 250–350 km vertical path (c) 250–350 km parabolic path.

#### 4.1.2. Ionospheric Disturbance Released by $H_2$ in Different Paths and Its Influence on Radio Wave Propagation Path

Because the diffusion rate of  $H_2$  and  $H_2O$  and the first reaction rate of ionic chemical reaction released to the ionosphere are inconsistent, the electron density dissipation degree and disturbance range are also inconsistent. The specific ionospheric disturbance and its impact on the radar radio wave propagation path are shown in Figures 3–6.

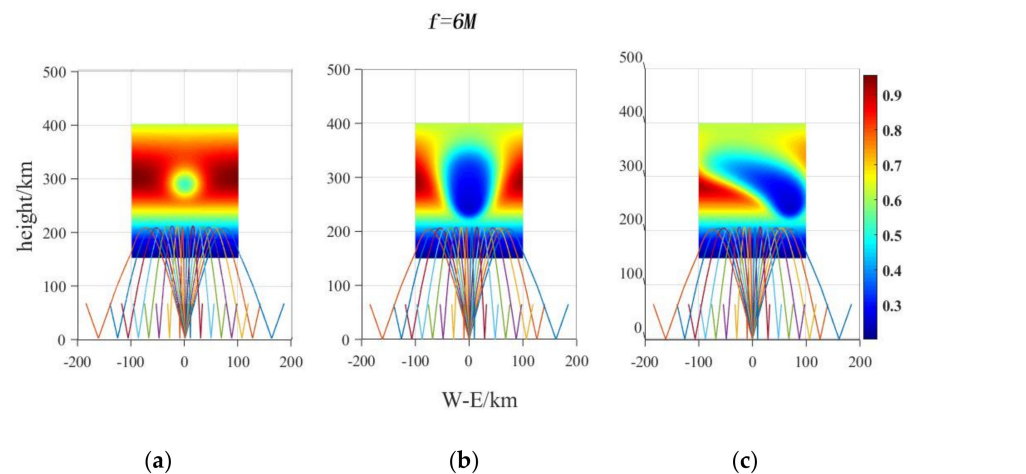


**Figure 3.** 3D ray-tracing simulation of 6 MHz short wave propagation path after 100 s of  $H_2$  released by rocket under different flight paths (electron density unit:  $10^6 \text{ cm}^{-3}$ ): (a) 300 km fixed-point release, (b) 250–350 km vertical path, (c) 250–350 km parabolic path.

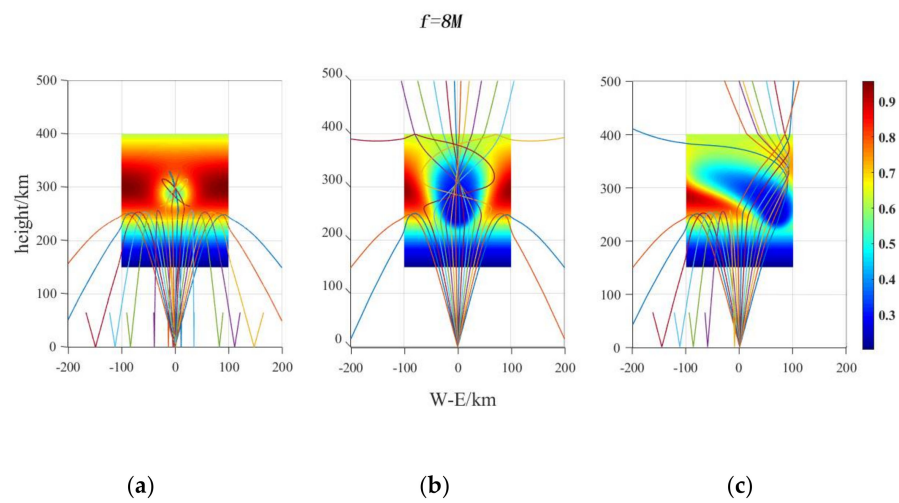


**Figure 4.** 3D ray-tracing simulation of 8 MHz short wave propagation path after 100 s of H<sub>2</sub> released by rocket under different flight paths (electron density unit: 10<sup>6</sup> cm<sup>-3</sup>): (a) 300 km fixed–point release, (b) 250–350 km vertical path, (c) 250–350 km parabolic path.

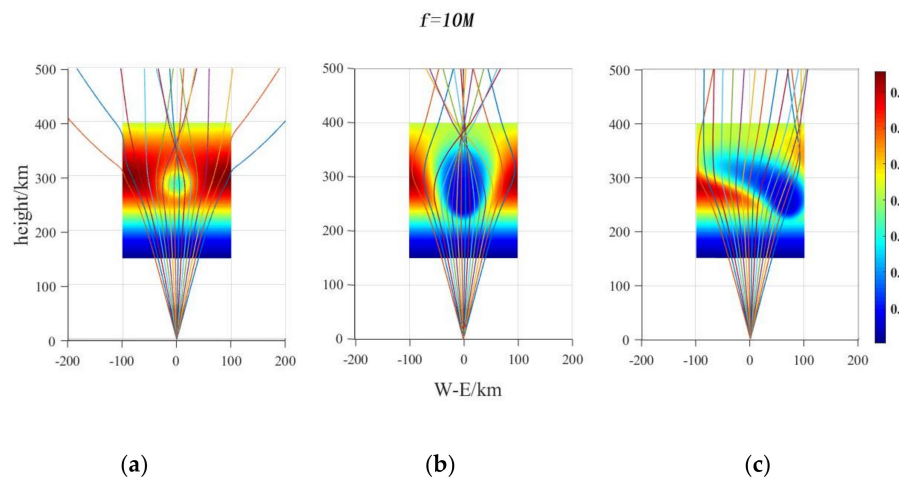


**Figure 5.** 3D ray-tracing simulation of 10 MHz short wave propagation path after 100 s of H<sub>2</sub> released by rocket under different flight paths (electron density unit: 10<sup>6</sup> cm<sup>-3</sup>): (a) 300 km fixed–point release, (b) 250–350 km vertical path, (c) 250–350 km parabolic path.

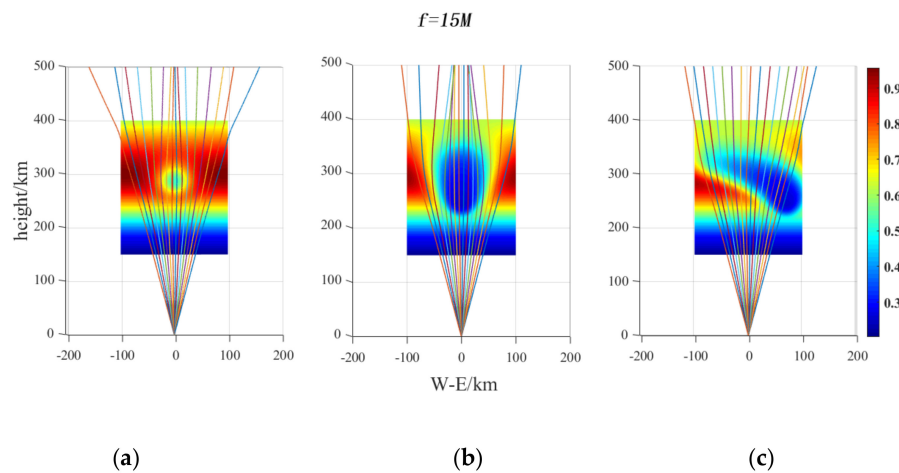


**Figure 6.** 3D ray-tracing simulation of 15 MHz short wave propagation path after 100 s of H<sub>2</sub> released by rocket under different flight paths (electron density unit: 10<sup>6</sup> cm<sup>-3</sup>): (a) 300 km fixed–point release (b) 250–350 km vertical path (c) 250–350 km parabolic path.

Figures 3, 4, 5 and 6a–c show the ionospheric disturbance generated by the rocket after releasing  $H_2$  for 100 s under different flight paths (i.e., fixed-point release at 300 km; vertical path at 250–350 km; parabola path at 250–350 km) and its influence on radar wave propagation at different frequencies. It can be seen from the figure that the shapes of ionospheric holes generated under different flight paths of the rocket are also different. After 3000 mol  $H_2$  is released at a fixed point of 300 km for 100 s, ellipsoidal ionospheric holes are generated. However, after releasing 3000 mol  $H_2$  every 5 km from 250 km to 350 km in the vertical direction for 100 s, a spindle ionospheric cavity is generated. After releasing 3000 mol  $H_2$  for 100 s on the parabolic curve path from 250 km to 350 km, a parabolic like ionospheric cavity structure is generated. As can be seen from Figures 3, 4, 5 and 6b, after the release of  $H_2$  for 100 s in the vertical path of 250–350 km, a spindle shaped ionospheric cavity is generated, and the maximum radius of the ionospheric cavity generated by the release of  $H_2$  reaches 56 km at the height of 320 km.

The vertical path and parabolic path release are continuous and multisource release, the release range and release amount are significantly larger than point source release, neutral gas molecules can react rapidly with ions and electrons in the ionosphere, consuming a large number of electrons in the ionosphere, so the resulting electron density depleting point source release is significantly lower than the vertical/parabolic path release.

Aiming at the different ionospheric cavity disturbance forms under different release paths, the influence of different ionospheric cavity disturbance forms on the radio wave propagation of sky wave radar is simulated by using 3D ray-tracing technology. As shown in Figure 3a–c, although the release of  $H_2$  through different paths to produce ellipsoidal, spindle and parabolic-like ionospheric cavities, the critical frequency at the bottom of the ionospheric cavity is greater than 6 MHz because the frequency of 6 MHz short wave is small and less than the critical frequency at the lower boundary of the cavity; in other words, the maximum reflection height of 6 MHz short wave is lower than the minimum disturbance height of the three forms of ionospheric cavity disturbance area, so 6 MHz short wave does not reach the height of the ionospheric disturbance area after incident, that is, it is reflected back to the ground. Therefore, three different forms of ionospheric cavity disturbance have no impact on the propagation of 6 MHz short wave.

Figure 4a–c shows the propagation path of 8 MHz short wave. It can be seen that 8 MHz short-wave beams pass through the lower boundary of three different forms of ionospheric holes. However, due to the weak ionospheric disturbance caused by fixed-point release in Figure 4a, 8 MHz beams with an elevation of nearly  $90^\circ$  can penetrate the lower boundary, but is not able to penetrate the upper boundary. After multiple reflections at the cavity boundary, it is finally reflected back to the ground. This is because the electron density at the upper boundary of the ionospheric cavity is greater than that at the lower boundary, so the 8 MHz short wave is greater than the critical frequency at the lower boundary and less than the critical frequency at the upper boundary. Therefore, it can penetrate the lower layer of the ionospheric cavity and is not able to penetrate the upper layer. Due to the large range of ionospheric holes generated by vertical release in Figure 4b, most 8 MHz short wave beams pass through the spindle ionospheric hole disturbance area, and electromagnetic wave focusing effect occurs, resulting a focus in the ionospheric hole. In contrast to the case of fixed-point release, in the case of vertical release, with the exception that two beams pass through the side boundary of the cavity after reflection, other beams passing through the bottom of the cavity pass through the top of the cavity, and the propagation of the beam presents an obvious symmetrical structure. Figure 4c shows the influence of parabolic ionospheric cavity on 8 MHz short wave propagation. The beam propagation presents obvious asymmetric characteristics. All beams in the east of the transmission point pass through the disturbance area, and after passing through, the focusing effect occurs on the upper part of the disturbance area, which completely changes the propagation direction of electric wave, and in some instances, the propagation direction is even or is completely opposite; all beams in the west of the transmitting point do not reach the disturbance area and are directly reflected to the ground. Figures 5 and 6a–c show

the propagation paths of 10 MHz and 15 MHz short wave. It is found that for three different forms of ionospheric cavity disturbance, the 10 MHz and 15 MHz beams completely pass through the ionospheric disturbance area and have different degrees of focusing effect. Moreover, it is found that the focusing effect of short wave passing through the ionospheric disturbance region is the strongest in vertical release, followed by fixed-point release, and the parabolic release is the weakest. It is found that the focusing effect decreases with the increase of the incident frequency, and the corresponding focus increases with the increase in the incident frequency.

In order to highlight the ionospheric region disturbed by the release of the rocket tail flame, we show the ionospheric background region with a height range of 150–400 km. At the same time, it is also to better show the change of the ray path so that the change path of rays above 400 km can be more clearly displayed.

#### 4.2. Disturbance Released by H<sub>2</sub>O in Different Paths and Its Influence on Radar Wave Propagation Path

Similarly, we simulate the ionospheric cavity formed by H<sub>2</sub>O under three different release conditions and its effect on radar wave propagation. Firstly, we simulated the release of 3000 mol H<sub>2</sub>O at a fixed altitude of 300 km; then, the release of 3000 mol H<sub>2</sub>O every 5 km from 250 km to 350 km when the rocket flies in a vertical path is simulated; finally, we simulated the release of 3000 mol H<sub>2</sub>O every 5 km on the parabolic path from 250 km to 350 km under the same flight conditions.

##### 4.2.1. Simulation of Spatial Distribution of H<sub>2</sub>O after Release and Diffusion in Different Paths

As shown in Figure 7, after releasing H<sub>2</sub>O for 100 s according to fixed-point release of 300 km, vertical path release of 250–350 km and parabolic curve path of 250–350 km, the released substance H<sub>2</sub>O has different spatial distribution characteristics. Similar to the case of H<sub>2</sub> under three different release paths, when it is released at a fixed point of 300 km, the east–west diffusion of H<sub>2</sub>O is farther than the vertical height, so a flat ellipsoidal release space is also generated; when the 250–350 km vertical path is released, the east–west diffusion of the release substance is smaller than the vertical diffusion, resulting in a slender cylindrical diffusion space with narrow bottom and wide top; when released on a parabolic path of 250–350 km, a parabolic tubular release space is generated. Different from the diffusion of H<sub>2</sub> under three different release paths, the diffusion range of H<sub>2</sub> is greater than that of H<sub>2</sub>O after 100 s of release, because the molecular weight and collision cross-sectional area of H<sub>2</sub> are small, so the diffusion rate of H<sub>2</sub> is higher than that of H<sub>2</sub>O.

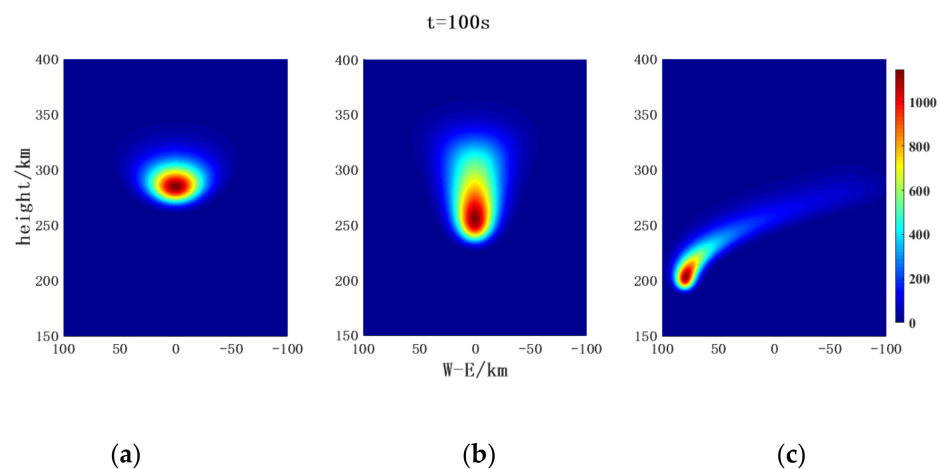


**Figure 7.** Spatial distribution of H<sub>2</sub>O released by rocket after releasing H<sub>2</sub>O for 100 s under different flight paths; (a) 300 km fixed–point release, (b) 250 km–350 km vertical path, (c) 250 km–350 km parabolic path (electron density unit: 10<sup>6</sup> cm<sup>−3</sup>).

#### 4.2.2. Ionospheric Disturbance Released by H<sub>2</sub>O in Different Paths and Its Influence on Radio Wave Propagation Path

Similarly, we simulated the ionospheric disturbance caused by H<sub>2</sub>O under three different release paths and its impact on the radar wave propagation path. The simulation results are shown in Figures 8–11.

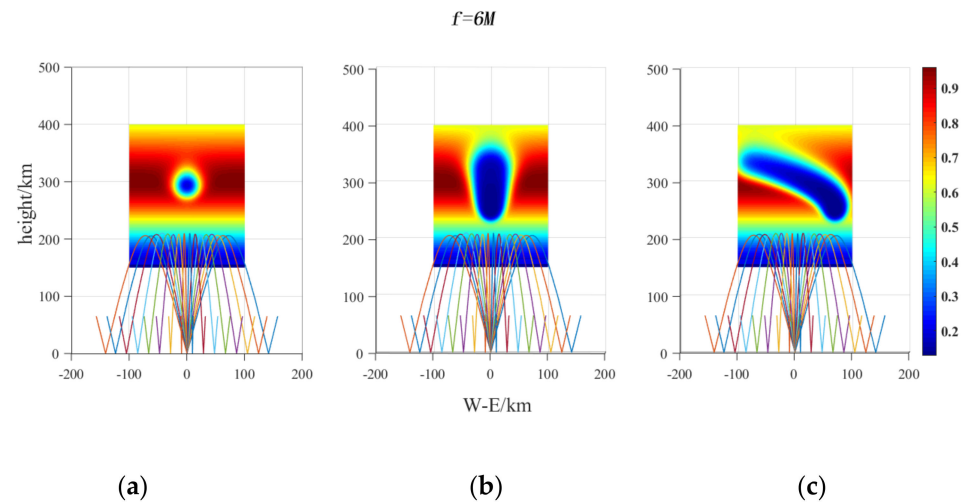


**Figure 8.** 3D ray-tracing simulation of 6 MHz short wave propagation path after 100 s of H<sub>2</sub>O released by rocket under different flight paths (electron density unit:  $10^6 \text{ cm}^{-3}$ ); (a) 300 km fixed-point release, (b) 250–350 km vertical path, (c) 250–350 km parabolic path.

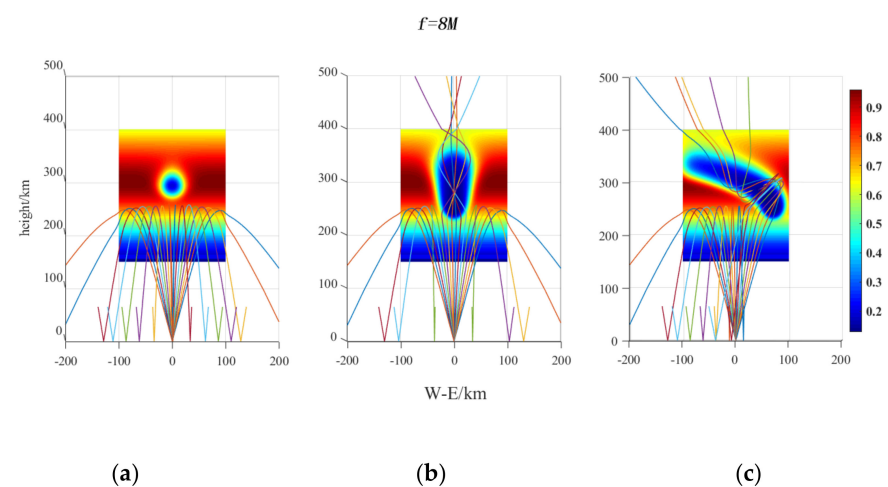


**Figure 9.** 3D ray-tracing simulation of 8 MHz short wave propagation path after 100 s of H<sub>2</sub>O released by rocket under different flight paths (electron density unit:  $10^6 \text{ cm}^{-3}$ ); (a) 300 km fixed-point release, (b) 250–350 km vertical path, (c) 250–350 km parabolic path.

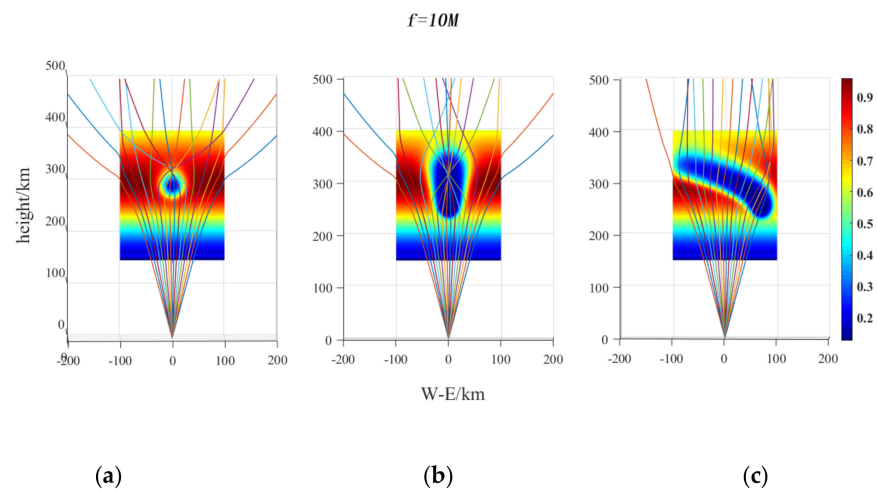


**Figure 10.** 3D ray-tracing simulation of 10 MHz short wave propagation path after 100 s of  $\text{H}_2\text{O}$  released by rocket under different flight paths (electron density unit:  $10^6 \text{ cm}^{-3}$ ); (a) 300 km fixed–point release, (b) 250–350 km vertical path, (c) 250–350 km parabolic path.

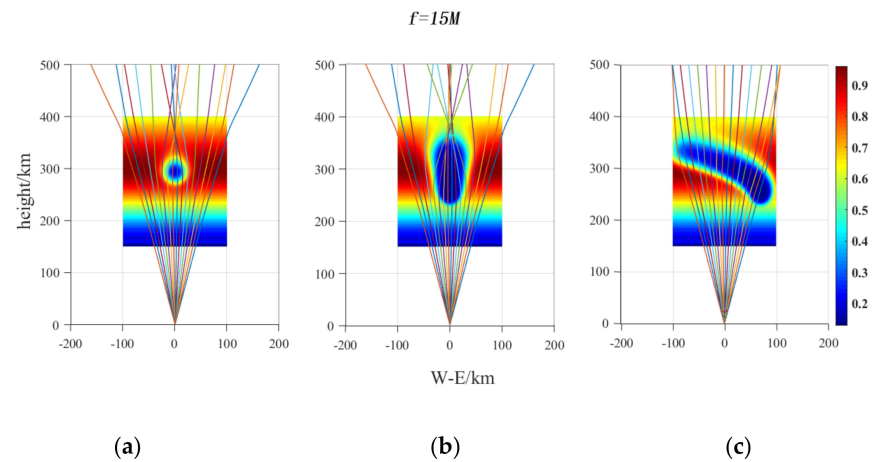


**Figure 11.** 3D ray-tracing simulation of 15 MHz short wave propagation path after 100 s of  $\text{H}_2\text{O}$  released by rocket under different flight paths (electron density unit:  $10^6 \text{ cm}^{-3}$ ); (a) 300 km fixed–point release, (b) 250–350 km vertical path, (c) 250–350 km parabolic path.

Figures 8, 9, 10 and 11a–c shows the ionospheric disturbance generated by the rocket after releasing  $\text{H}_2\text{O}$  for 100 s under different flight paths (i.e., fixed-point release at 300 km; vertical path at 250–350 km; parabola path at 250–350 km) and its impact on radar wave propagation at different frequencies. Similar to the ionospheric disturbance generated by  $\text{H}_2$  under the same release path, an ellipsoidal ionospheric cavity is generated after releasing 3000 mol  $\text{H}_2\text{O}$  at a fixed point of 300 km for 100 s. After releasing 3000 mol  $\text{H}_2\text{O}$  every 5 km in the vertical direction from 250 km to 350 km for 100 s, a spindle ionospheric cavity is generated. After releasing 3000 mol  $\text{H}_2\text{O}$  for 100 s on the parabolic curve path from 250 km to 350 km, a parabolic-like ionospheric cavity structure is generated. Compared with the ionospheric disturbance generated by  $\text{H}_2$  under the same release path, the basic shape of the ionospheric cavity generated by  $\text{H}_2\text{O}$  under the same release path is essentially consistent with the ionospheric disturbance generated by releasing  $\text{H}_2$ . However, the ionospheric disturbance range produced by  $\text{H}_2$  is larger than that produced by  $\text{H}_2\text{O}$ . The dissipation degree of ionospheric electron density caused by the release of  $\text{H}_2\text{O}$  is higher than that produced by  $\text{H}_2$ , and the maximum relative change rate of electron density is greater. In addition, the boundary of the ionospheric cavity produced by the release of  $\text{H}_2\text{O}$  is clearer and less gradual than that produced by the release of  $\text{H}_2$ , while the level of electron density disturbance at the boundary is not very obvious.

Aiming at the different ionospheric cavity disturbance forms under different release paths, the influence of different ionospheric cavity disturbance forms on the radio wave propagation of sky wave radar is simulated by using three-dimensional ray-tracing technology. As shown in Figure 8a–c, it is also similar to the case of H<sub>2</sub> release under different paths. Because the frequency of 6 MHz short wave is small and less than the critical frequency of the lower boundary of the cavity, all 6 MHz short waves are reflected back to the ground without reaching the height of the ionospheric disturbance area after incident. The three different forms of ionospheric cavity disturbances produced by the release of H<sub>2</sub>O also have no effect on the propagation of 6 MHz short wave.

For the propagation path of 8 MHz short wave, it can be seen from Figure 9a that in contrast with the case of releasing H<sub>2</sub> at a fixed point of 300 km, when releasing H<sub>2</sub>O at a fixed point of 300 km, due to the slow diffusion rate of H<sub>2</sub>O and small disturbance range, 8 MHz short wave is reflected back to the ground without reaching the lower boundary of ionospheric cavity. It can be seen from Figure 9b, in contrast with the case of releasing H<sub>2</sub> in the vertical path, due to the slow diffusion rate of released H<sub>2</sub>O and small disturbance range, only the 8 MHz beam with the elevation angle closest to 90° can pass through the ionospheric cavity, while most 8 MHz short-wave beams are reflected back to the ground without reaching the ionospheric disturbance area. Compared with Figures 4c and 9c, when the parabolic path is released, the propagation path of 8 MHz short wave beam is also different because the diffusion rate of released H<sub>2</sub>O is slow and the disturbance range is small, but the electron density dissipation degree is deep and the electron density gradient is large. Figure 9c shows the influence of the parabolic ionospheric cavity on the 8 MHz short wave propagation. The beam propagation presents obvious asymmetric characteristics. The 8 MHz short wave beam in the east of the emission point passes through the ionospheric cavity after multiple reflections at the inner boundary of the parabolic ionospheric cavity and changes the propagation direction of the radio wave to a great extent. All beams in the west of the transmitting point do not reach the disturbance area and are directly reflected back to the ground.

Figures 10 and 11a–c show the propagation paths of 10 MHz and 15 MHz short waves, which are also similar to the influence of three different forms of ionospheric cavity disturbance generated when H<sub>2</sub> is released on 10 MHz and 15 MHz short waves under the same conditions. The beams of the two frequencies completely pass through the ionospheric disturbance area and have different degrees of focusing effect. Similar to the case of H<sub>2</sub> release, the ionospheric disturbance area generated during vertical release affects the most beams, the focusing effect of radio waves is the strongest and the fixed-point release is the second, while the parabolic release is the weakest. The focusing effect decreases with the increase in the incident frequency, and the corresponding focus increases with the increase in the incident frequency.

## 5. Conclusions

The main purpose of this paper is to study the disturbance of the ionosphere caused by the release of neutral gases from the rocket plume. For chemical substances H<sub>2</sub> and H<sub>2</sub>O, there is a process of generating ionospheric disturbance under three different release conditions: 300 km fixed-point release, 250–350 km vertical path and 250–350 km parabolic path. Finally, the path changes of high-frequency radio waves of different frequencies through the disturbed ionosphere are obtained through simulation.

In this study, we considered the neutral gas diffusion process, ion chemical reaction and plasma diffusion process; a three-dimensional dynamic model is developed to obtain the electron density of ionospheric and the temporal and spatial distribution of rocket plume plasma. At the same time, the modeling parameters, such as the initial neutral atmospheric, background ionospheric, and geomagnetic field configuration, were obtained from the NRLMSISE-00 model, the international reference ionospheric 2016 (IRI-2016) model, and the IGRF-13 model, respectively.

In addition, 3D digital ray-tracing technology is used to simulate the influence of ionospheric cavity produced by neutral gas released by rocket plume on the echo path of high frequency radio waves with different incident frequencies is simulated. A fast algorithm is used in the simulation, and the group path step size is adjusted adaptively according to the gradient of plasma frequency.

The main findings about the propagation effects of radio waves are as follows:

The focusing effect of short wave passing through the ionospheric disturbance region is the strongest in vertical release, followed by fixed-point release, and the focusing effect of radio waves is the weakest in parabolic release. In the future, we will consider the effect of ionospheric irregularities on radio wave propagation in subsequent works.

**Author Contributions:** Conceptualization, Q.L. and Z.L.; methodology, Q.L.; software, Z.L.; validation, Q.L. and H.F.; formal analysis, Q.L.; investigation, Q.L.; resources, H.F.; data curation, Q.L. and Z.L.; writing—original draft preparation, Q.L.; writing—review and editing, H.F.; visualization, Q.L.; supervision, H.F.; project administration, H.F.; funding acquisition, H.F. All authors have read and agreed to the published version of the manuscript.

**Funding:** This research was funded by Hanxian Fang grant number 41804149 And The APC was funded by Hanxian Fang.

**Institutional Review Board Statement:** Not applicable.

**Informed Consent Statement:** Not applicable.

**Data Availability Statement:** The data in this study mainly used NRLMSISE-00, IRI-2016 and IGRF-13 model parameter data. NRLMSISE-00 data, IRI data and IGRF-13 data can obtain from <https://ccmc.gsfc.nasa.gov/modelweb/models/nrlmsise00.php>, [https://ccmc.gsfc.nasa.gov/modelweb/models/iri2016\\_vitmo.php](https://ccmc.gsfc.nasa.gov/modelweb/models/iri2016_vitmo.php) and [https://ccmc.gsfc.nasa.gov/modelweb/models/igrf\\_vitmo.php](https://ccmc.gsfc.nasa.gov/modelweb/models/igrf_vitmo.php), respectively (all accessed on 10 May 2022).

**Conflicts of Interest:** The authors declare no conflict of interest.

## References

- Booker, H. A local reduction of F-region ionization due to missile transit. *J. Geophys. Res.* **1961**, *66*, 1073–1079. [[CrossRef](#)]
- Mendillo, M.; Hawkins, G.S.; Klobuchar, J.A. A Large-Scale Hole in the Ionosphere Caused by the Launch of Skylab. *Science* **1975**, *187*, 343–346. [[CrossRef](#)] [[PubMed](#)]
- Mendillo, M.; Hawkins, G.S.; Klobuchar, J.A. A sudden vanishing of the ionospheric F region due to the launch of Skylab. *J. Geophys. Res. Atmos.* **1975**, *80*, 2217–2228. [[CrossRef](#)]
- Zinn, J.; Sutherland, C.D.; Stone, S.N.; Duncan, L.M.; Behnke, R. Ionospheric effects of rocket exhaust products—heacoc, skylab. *J. Atmos. Sol.-Terr. Phys.* **1982**, *44*, 1143–1171. [[CrossRef](#)]
- Savastano, G.; Komjathy, A.; Shume, E.; Vergados, P.; Ravanelli, M.; Verkhoglyadova, O.; Meng, X.; Crespi, M.G. Advantages of Geostationary Satellites for Ionospheric Anomaly Studies: Ionospheric Plasma Depletion Following a Rocket Launch. *Remote Sens.* **2019**, *11*, 1734. [[CrossRef](#)]
- Zhao, H.-S.; Feng, J.; Xu, Z.-W.; Wu, J.; Wu, Z.-S.; Xu, B.; Xue, K.; Xu, T.; Hu, Y.-L. A temporal three-dimensional simulation of samarium release in the ionosphere. *J. Geophys. Res. Space Phys.* **2016**, *121*, 10508–10519. [[CrossRef](#)]
- Zhao, H.; Xu, Z.W.; Tang, W.; Xu, Z.-H.; Xue, K.; Xie, S.; Zheng, Y.; Wu, J.; Zhang, J.-D. Electromagnetic scattering by artificial plasma clouds in the ionosphere. *IEEE Trans. Antennas Propag.* **2020**, *68*, 4810–4819. [[CrossRef](#)]
- Croft, T.A.; Hoogasian, H. Exact ray calculations in a quasi-parabolic ionosphere with no magnetic field. *Radio Sci.* **1968**, *3*, 69–74. [[CrossRef](#)]
- Davies, K.; Rush, C.M. High-frequency ray paths in ionospheric layers with horizontal gradients. *Radio Sci.* **1985**, *20*, 95–110. [[CrossRef](#)]
- Dyson, P.L.; Bennett, J.A. A model of the vertical distribution of the electron concentration in the ionosphere and its application to oblique propagation studies. *J. Atmos. Terr. Phys.* **1988**, *50*, 251–262. [[CrossRef](#)]
- Norman, R.J.; Cannon, P.S. A two-dimensional analytic ray tracing technique accommodating horizontal gradients. *Radio Sci.* **1997**, *32*, 387–396. [[CrossRef](#)]
- Haselgrove, J. *Ray Theory and a New Method of Ray Tracing*; The Physical Society: London, UK, 1955; Volume 23, pp. 355–360.
- Jones, R.M. A three-dimensional ray-tracing computer program. *Radio Sci.* **1968**, *3*, 93–94. [[CrossRef](#)]
- Kelso, J.M. Ray Tracing in the ionosphere. *Radio Sci.* **1968**, *3*, 1–12. [[CrossRef](#)]
- Zhou, C.; Zhao, Z.; Deng, F. Effects of the travelling ionospheric disturbance on skywave over-the-horizon radar coordinate registration. *Syst. Eng. Electron.* **2011**, *33*, 2222–2225. [[CrossRef](#)]

16. Hu, Y.G.; Zhao, Z.Y.; Zhang, Y.N. Ionospheric disturbances produced by chemical releases and the resultant effects on short-wave ionospheric propagation. *J. Geophys. Res.* **2011**, *116*, 395–402. [[CrossRef](#)]
17. Schunk, R.W.; Szuszczewicz, E.P. Plasma expansion characteristics of ionized clouds in the ionosphere: Macroscopic formulation. *J. Geophys. Res.* **1991**, *96*, 1337–1349. [[CrossRef](#)]
18. Hu, Y.G.; Zhao, Z.Y.; Zhang, Y.N. Study on ionospheric release effects of several typical chemicals. *Acta Phys. Sin.* **2010**, *59*, 8293–8303.
19. Gatsonis, N.A.; Hastings, D.E. A three-dimensional model and initial time numerical simulation for an artificial plasma cloud in the ionosphere. *J. Geophys. Res.* **1991**, *96*, 7623–7639. [[CrossRef](#)]
20. Mendillo, M.; Semeter, J.; Noto, J. Finite element simulation (FES): A computer modeling technique for studies of chemical modification of the ionosphere. *Adv. Space Res.* **1993**, *13*, 55–64. [[CrossRef](#)]
21. Wang, Y. A Study on Ionospheric Effect of the Rocket Plume. Master's Thesis, Wuhan University, Wuhan, China, 2008.
22. Ferguson, E.E. Rate constants of thermal energy binary ion-molecule reactions of aeronomic interest. *At. Data Nucl. Data Tables* **1973**, *12*, 159–178. [[CrossRef](#)]
23. Anderson, D.N.; Bernhardt, P.A. Modeling the effects of an H<sub>2</sub> gas release on the equatorial ionosphere. *J. Geophys. Res. Space Phys.* **1978**, *83*, 4777–4790. [[CrossRef](#)]